Wavefront Signal Extraction and TCS

E. Calloni[1,2], M. Laval[3] , J. Marque[4] , P. Ruggi[4].

1: Università Federico II di Napoli, Complesso Universitario Monte Sant' Angelo, via Cinthia, Naples, Italy

2: INFN, sez. di Napoli, Complesso Universitario Monte Sant' Angelo, via Cinthia, Naples, Italy

3: Observatoire de la Cte d'Azur ARTEMIS, UMR OCA/CNRS B.P. 4229, 06304 NICE Cedex 4 FRANCE

4: EGO - European Gravitational Observatory - Cascina, Pisa, Italy

Abstract

The behavior of the beams wavefronts in the different sections of the interferometer is an important subject for the understanding of the interferometer behavior and for an efficient compensation of thermal lensing effect. In this note we present the status of the art of wavefront simulations and measurements. Different approaches to TCS error signal extraction will be addressed.

Introduction

The behavior of the beams' wavefronts inside the interferometer is a subject of interest both for the generation of an efficient error signal for Thermal Compensation System and for the understanding of major features of the present and future detectors. In particular, as it is known, while the carrier typically exhibits a simple geometrical shape, this is not the case for the sidebands which, not being resonating in the long arms, are highly affected by the aberrations of the mirrors of the unstable recycling cavity. Generally the highest perturbations are due to thermal effects on the input mirrors, and a major effort is being carried on in describing the resulting sidebands aberrations and designing an efficient TCS to correct them. Long and interesting works on sidebands behavior have been already carrier out by J. Marque [1] and M. Laval [2], working with the simulation codes Finesse and DarkF, and interesting results have been obtained especially regarding the possible use of the Nominal modulation frequency frequency instead of Anderson one. In this note particular attention will be posed to the phase camera0 signals, their dependence on sidebands aberrarations, and on their possible use as error signal for thermal compensation. The problem of error signal extraction for TCS will be addressed and discussed pointing out the points still under discussion. The note is organized as follows. In section 1 the most important measurements are presented, especially with respect to thermal transient. Then section 2 is devoted to results of DarkF and Finesse simulations, some analytical calculations and conclusions. The details of calcutations are reported in Appendix. The results will be compared with the relative measurements and in the concluding section they will be used to indicate the signals presently foreseen as TCS error signals.

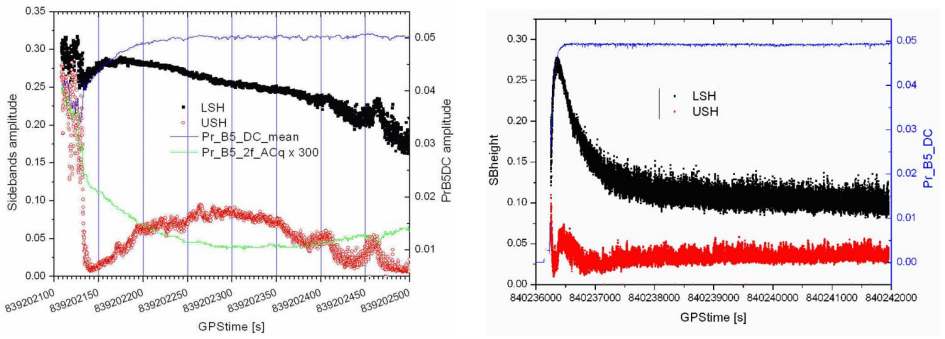

Figura 1: Short-Term and Long-Term carrier and sidebands thermal evolutions. It is noted the different effect that thermal lensing produces on the Carrier, Upper Sideband and Lower sideband recycling gains

1 Measurements of geometrical sidebands behavior

1.1 Sidebands gains versus Michelson alignment

The thermal behavior of sidebands gains is reported in figure 1. at the beginning of the lock $G_{Carrier} = 40$, $G_{Sidebands} = 30$, and after thermal stabilization $G_{Carrier} = 41$, $G_{Sidebands} = 11$. Note that the final value of sidebands recycling gain is achieved after a tuning of PRCL which indeed equalizes the powers. The different dependence of the three powers from the thermal lensing is shown: the carrier is essentially not affected by the input mirror deformation, the Lower sidebands is quite affected by the deformation and the Upper sidebands is deeply affected. The explanation of this effects will be given in the section devoted to DarkF simulations. Once the interferometer is completely locked and the thermal lensing has reached a stationary condition the sidebands are equalized by adding suitable off-sets to the length of the recycling cavity. A consequence of the different behavior of the two sidebands, which is a clear prove of the (not intuitive) importance of the phase the sidebands

acquire in the *long-arms* (see in next section), is the dependence of the differential sidebands power by Michelson alignment. Due to Anderson Technique, a different reflection law for the sidebands and carrier is the expected, as shown in figure 2. In particular the Upper sideband and the carrier are reflected backwards, while the lower sideband follows the usual specular reflection. This different behavior couple a tilt (of the input beam) with sidebands un-balancing.

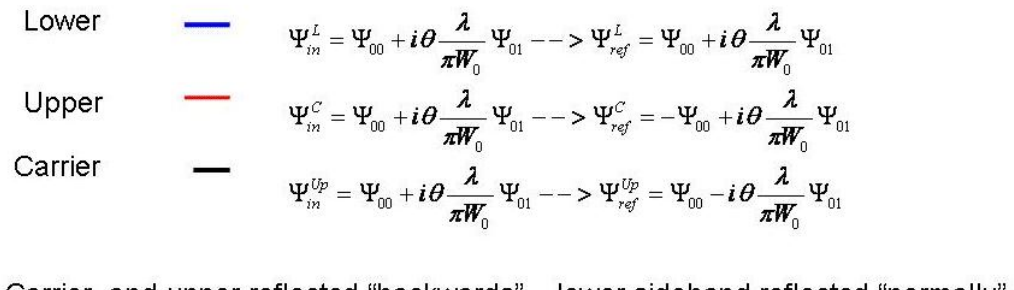

Figura 2: The reflection from a cavity, due to Anderson Technique is different for the two sidebands, as shown by the first order calculation. The Upper sideband follows the carrier while the Lower sideband follows the usual reflection law

Measurements have been carried to put in evidence this effect and eventually to relate it to a search for better alignment condition. The input beam is tilted in $theta_x$ by adding an off-set to a BMS error signal and compensate the induced translation

(read by B5) adding an off-set on the other BMS error signal. We observe the expected un-balancing of the sidebands that we correct adding an off-set (manually) on the longitudinal degree of B2. We obtain, as a result, that working with a negative off-set in $theta_x$ the longitudinal off-set needed to balance the sidebands is lowered (a good off-set is about -0.7). Working in this new point does not worst the sensitivity and further experiment should be done to clarify if it gets better: there is a noise lowering (to be confirmed) in structures due to jitter noise (190 Hz - 206 Hz) that suggests that this working point corresponds to a better alignment and, in our opinion, that this condition should be further investigated. Working around this point allows to enhance the region of longitudinal off-sets that can be explored to search for best locking conditions.

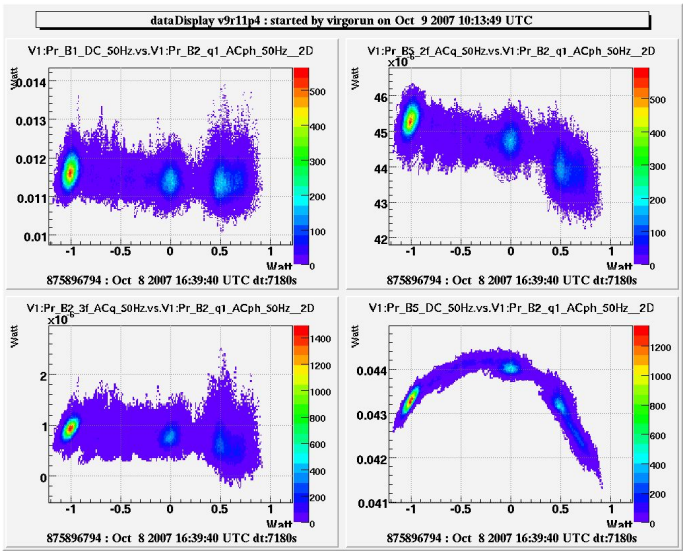

Figura 3: The region of negative off-set in alignment, once the sidebands unbalancing is corrected by the off-set on B5, shows a higher sidebands' gain. Around the value -0.7 the input beam alignment should be tested to prove the reaching of a better alignment. The not negligible lowering of the carrier put the interferometer in a lower robust condition.

The sidebands gain is enhanced in this region while the carrier gain lowers so that

finally, working around this positions, lowers the robustness of the interferometer. A possibility to rise again the carrier gain could be to add an off-set to the CARM loop, to end with an interferometer with higher sidebands gain and usual carrier gain. Nonetheless this studies would requires quite long studies and long dedicated time. The present decision is then to not cure the low sidebands gains by exploring the (now higher) allowed off-sets region but by directly with the master way of TCS.

1.2 Measurements with the phase camera

The effect of thermal lensing is ubiquitous in Virgo signals. Nonetheless, in the majority of them, it is superposed to other typical imperfections, like misalignments. In order to extract a clear error signal to feed the Thermal Compensation System (TCS) a phase camera have been built. It consists in a pin-hole placed in front of a photodiode (which let pass a small fraction of the wavefront) and of a scanning system that allows to span all the wavefront. The analyzed beam is B5 and the photodiode current is demodulated at the Virgo modulation frequency Ω_m, in phase (This choice is justified later in the note, in the analytical simulation section). The result of the measurement in cold interferometer are shown in figure 4 where an astigmatism of the input beam is detected. The amplitude of this astigmatic term is approximatively the 15/100 of the fundamental mode, in agreement with the 3/100 power value previously measured in transmission through t the arm cavities.

The thermal evolution of the wavefront is represented in figure 5 . During the transient the astigmatic term decreases and the first Laguerre-Gauss mode, called *defocus*, increases and finally remains the dominant term. While the final status of the wavefront is in very good agreement with the expected one (see section on DarkF simulation) it remains unclear why the astigmatic term decreases. Unfortunately,

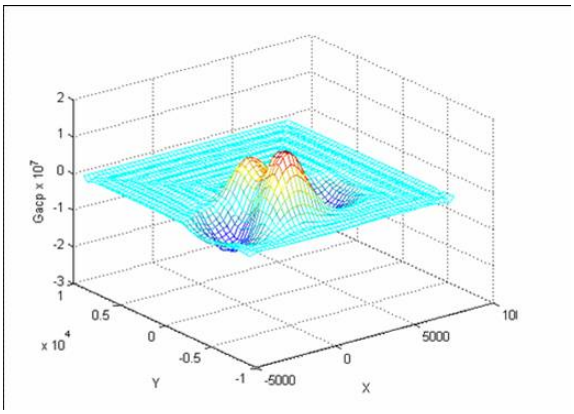

Figura 4: Phase Camera signal just after lock acquisition. The wavefront is astigmatic

at the moment, DarkF does not allow to enter the interferometer with an aberrated beam. It is presently planned a suitable analysis with Finesse.

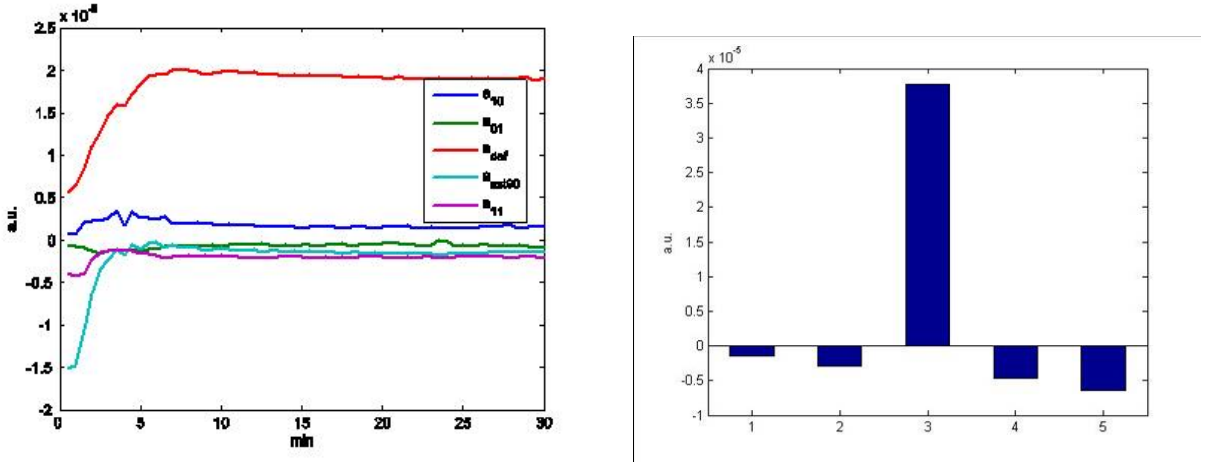

Figura 5: Left: Thermal evolution of the aberrations of sidebands wavefront. The red curve is the defocus term, growing as expected due to thermal lensing of input mirrors. Right: Final Status, showing the relative mode composition at the end of thermal transient.

The final picture of wavefront is reported in figure 6. The mode is practically a Laguerre-Gauss mode, as expected. The clear dependence of this signal from the input mirrors radii of curvature variations could make it a suitable error signal for

TCS; in particular we point out that thanks to the work carried out by D. Sentenac, the modes reconstruction can be done on-line. Nonetheless, at the present, the decision is to not have the PZT running during Science Mode, because it could be a source of noise.

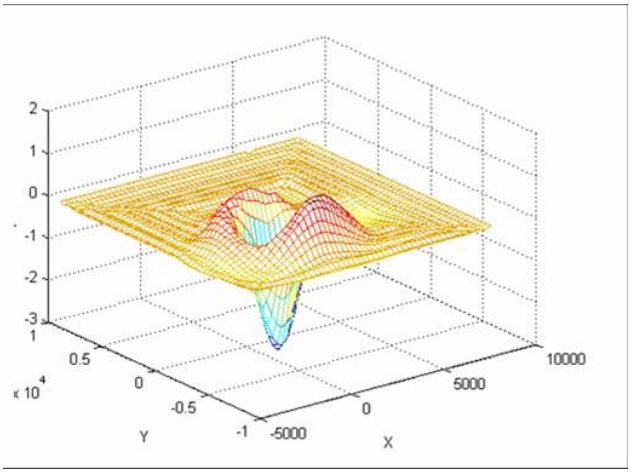

Figura 6: iii

For this reason this signal will be used, extensively, only during the tests of TCS, to measure its efficiency and purity (i.e. to avoid reintroducing other aberration like astigmatisms). In Science Mode the signal will be built with a bull'eye-equivalent photodiode system, made of a pin-hole mirror and a couple of photodiode, like in figure 7, which is sensitive to the first Laguerre-Gauss mode.

The TCS must compensate two mirrors defocus so that, strictly speaking, two error signal should be provided to for the feed-back. Nonetheless it is still questionable if there is the real need of two signals, for the mirrors behavior is well known: they are heated by the same amount of laser light, the relative absorption constants are well known, the temporal behavior is the same. Furthermore the Ligo experience shows that a single error signal should be sufficient. The phase camera signal,

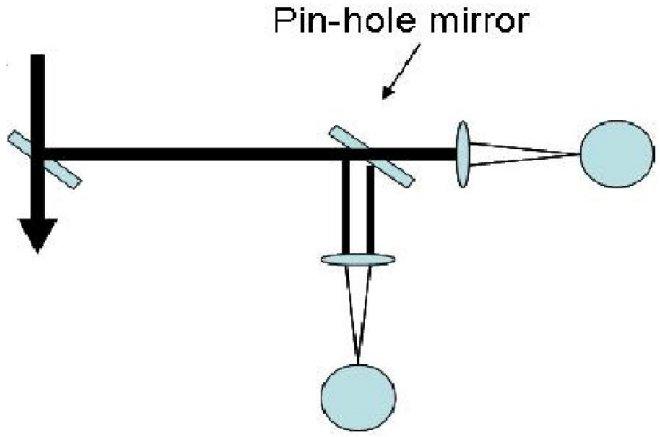

Figura 7: The pin-hole mirror system: the beam analyzed is B5; the signal is given by the difference of the two photodiodes, demodulated at Ω_m, and it is proportional to the first Laguerre-Gauss mode

detecting the mean sidebands wavefront with respect to the carrier, is a common mode signal of the two mirrors defocusing. The best candidate for the differential is $B1p_Acq$, (also used in Ligo when firstly two signals where used) which is the signature of the not superposition of the sidebands. Presently a final decision on the second error signal is not be taken; further simulations are expected.

2 Simulations

The fields inside the interferometer have not all an intuitive behavior. Indeed, while the carrier maintains its shape also in presence of thermal lensing, the sidebands exhibit a non trivial dependence from interferometer imperfections. For these reason a careful simulation of the interferometer is mandatory, together with a correct intuitive description, if possible. As it is known, presently Virgo can be simulated with two different tools: DarkF and Finesse. The first is a code performing the diffraction propagation without the use of mode description. For this reason is

very general and can take into account the aberration maps of the optics (i.e. the point-like measured refraction index and absorption of the mirrors). The complexity of the simulation method does not allow the simulation of imperfect input beams, and it cannot take into account interferometer misalignments. Finesse uses the mode expansion, so it is very flexible and suitable to describe aberrations that not require a too high order of mode to be described. For these reasons it cannot take into account the mirror maps but, on the other hand, it can easily describe low order imperfections like defocus, misalignments and so on. Both codes simulate the equilibrium state of the light in the interferometer, i.e. they cannot describe light transients. The simulations of sidebands behavior inside the interferometer has been object of studies in many respect, not only within the Optical Characterization or TCS error signal generation. In this attention is pointed out on some description useful for understanding that behavior and mostly for TCS error signal generation.

2.1 Mode-Cleaning effect of long arms

Extensive studies on thermal effect on the interferometer fields have been carried out thanks to M. Laval and J. Marque and the results are reported in various talks and notes. Within this note the progress with respect to previous works regards a pointing out of the eventual sideband mode cleaning by long arms and a more detailed simulations of TCS signals. The first effect simply due to the fact that, a bit contrary to intuition, even if the sidebands are not resonating in the arm cavities, their behavior is strongly dependent upon the phase acquired in the long arms.
To put in evidence this effect a particular modulation can be taken into account, i.e. the modulation at the frequency that makes a sideband resonating with the modes of order two of long arms. In this condition the mode-cleaning effect of the cavity

is maximum and can be explained in the following way: let us consider a perfect beam impinging on a mirror whose substrate has been deformed by thermal effcts. The predominant term is the lens effects that tends to focus the beam before being reflected from the coated surface. This situation is shown by the following formulas: let us suppose that the perfect ψ_{00} mode field of the sideband Ψ_{in}, of amplitude E_0 is impinging on the input mirror. Due to the lens effect the sideband will be slighlty focused and, before reflecting on the input mirror reflecting surface, the field Ψ_{imp} it will be

$$\Psi_{imp}^{USB} \approx E_0 \left[\psi_{00} + \imath A_{def} \left(\frac{\psi_{02} + \psi_{20}}{\sqrt{2}} \right) \right] \tag{1}$$

Note that f is the equivalent focal lenght of the warm substrate. The mode $\frac{\psi_{02}+\psi_{20}}{\sqrt{2}}$ is the Laguerre-Gauss mode L_{10}. In the following we do not move in the Laguerre-Gauss basis to be consistent with the Virgo praxis. This beam is converging, as denoted by the positive sign of the imaginary part of the mode amplitude $A_{def} = \frac{piW_0^2}{2\lambda f}$, concordant with the sign of ψ_{00} mode amplitude. The reflection of this field from the cavity can be approximated taken into account that the fundamental mode is not resonant with the cavity (remember that this is a sideband) while the high order mode of order two are resonant. Thus the field reflected from the cavity Ψ_{lea}, leaving the coated surface can be approximated as:

$$\Psi_{lea}^{USB} \approx E_0 \left[\psi_{00} - \imath A_{def} \left(\frac{\psi_{02} + \psi_{20}}{\sqrt{2}} \right) \right] \tag{2}$$

Here it must be noted the opposite sign between the amplitude of ψ_{00} mode and the amplitude of the imaginary part of Laguerre-Gauss mode: thus beam beam leaving the coated surface is diverging, exatcly of the same amount for it was converging. This beam, passing again on the substrate, will be again focused by the substrate, adding an imaginary part exaclty equal to the negative imaginary part now present.

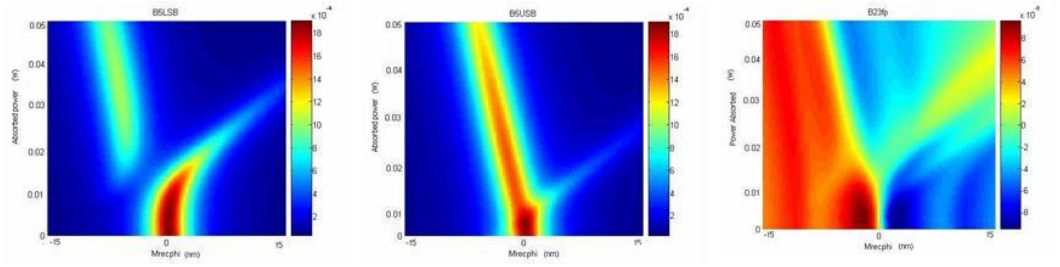

Figura 8: Sidebands power and B23f signal evolution as the absorbed power is increased. The upper sideband is not resonant with modes or order two of the arm cavity. Both the sidebands are affected by the rising of aberration

So finally the beam will leave the mirror being not aberrated, to the first order. This situation has been simulated by the use of Finesse. To be definite let us consider to modulate the beam at the frequency 6.282700 MHz: in this condition the upper sideband modes of order two are resonating in the long arms. For sake of simplicity the system considered is a double cavity system. As described in a previous note by J. Marque, a clear indication of the sidebands behaviour in presence of thermal aberrations can be obtained by simulating the system with the long arm's loop maintained closed (so that the long arm is in resonance with the carrier) and exploring the sidebands power while the Recycling mirror position is varied and the thermal aberrations taken into account. In general three-dimensional graphs are obtained, as in fig 8. On the X axis the Power Recycling mirror position is reported, on the Y axis the absorbed power and on the Z axis the power of the sidebands. For sake of completeness in fig 3 a third graph, the amplitude of the B23f error signal, is reported, showing the rising of a double stability point as the aberrations increase. (This figure has been carefully commented elsewhere by J.Marque).

If the none of the sidebands has the modulation frequency indicated above, the typical graphs of figure 8 are obtained, where both the sidebands power decrese

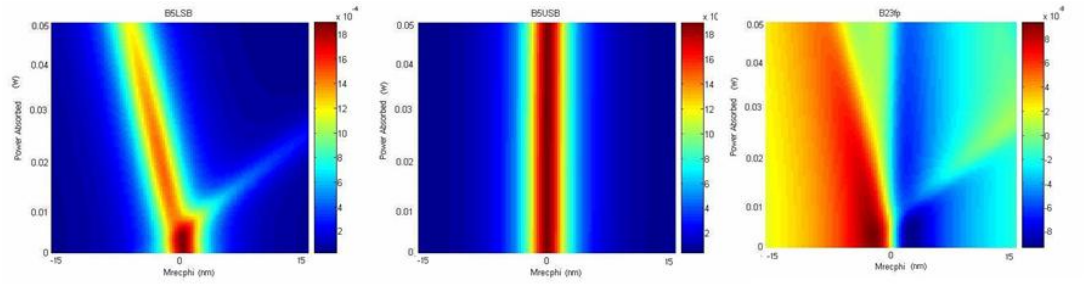

Figura 9: Sidebands power and B23f signal evolution as the absorbed power is increased. The upper sideband is resonant with modes or order two of the arm cavity. It is seen that it is almost not affected by the rising of aberration

as the aberrations grow. (Note that in particular the fig 3 refers to the Anderson modulation technique.) On the contrary, if the modulation frequency is chosen as described above, the power of the Upper Sideband does not decrease, as clearly seen in fig 9. We remark here that for the moment the use of this modulation frequency is not proposed and this study has to be considered as a view in understanding how the long arms can clean not only the carrier but also the (a) sideband in particular conditions.

Turning back to the present case and to the whole interferometer, considering that the modulation frequency is chosen such that the Upper sideband satisfies the Anderson condition (TEM01 mode resonating in the long cavities) and that the Lower sideband frequency is not resonant with any high order modes, the response of a sideband to an interferometer imperfection tends to be very different. In particular, the Upper sidebands of order 1 (misalignments) tends to be cleaned by the long arms (without cleaning the others) while the Lower sidebands order 1 are not at all cleaned by the arms. As shown in figure 10, where the cold interferometer is considered, the Lower sideband tends to be cleaned in the high order terms. The interferometer is cold, so the aberrations are small with respect to thermally driven condition. It is

visible the flatness of the Lower sideband wavefront (whose high order modes tend to be cleaned) which is nonetheless tilted. On the contrary, the Upper sidebands is not tilted but its wavefront is quite curved.

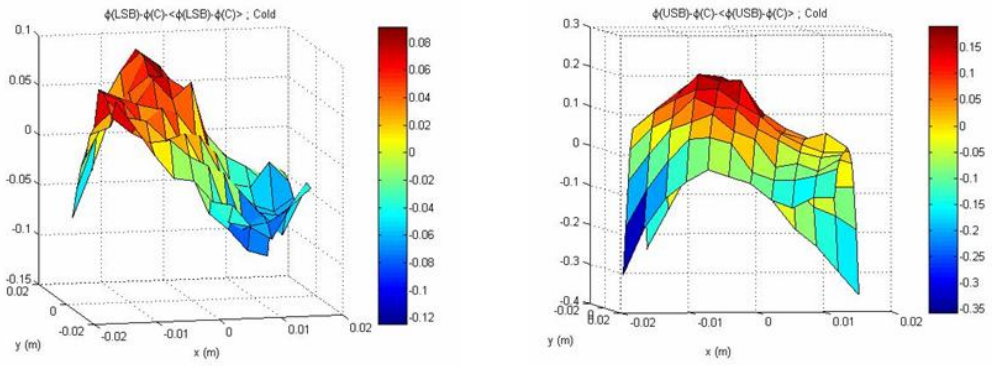

Figura 10: The simulation of the sidebands in cold interferometer. As expected the aberrations are quite low but illustrate the typical sidebands response to interferometer aberrations: the Lower sidebands, on the left, is more affected by misalignment for its wavefront its almost flat but tilted. On the contrary the Upper sideband, on the right, is less affected by misalignment, being cleaned by the Anderson condition, but it is curved, being more sensitive to high order aberrations, like defocus

These different conditions would explain at least the different temporal behavior of the two sidebands during the very first warming of the interferometer, as shown in figure 1: when the input mirrors acquire a lens effect that tends to curve the wavefronts, the Upper sidebands is not at all cleaned by the long arms and very quickly loses the resonance. The Lower sideband, cleaned with better efficiency on these modes, does not lose immediately its shape, and better fulfills the resonant conditions in the recycling cavity. On the contrary, the subsequent behavior of the interferometer is not still completely described by simulations as it needs a careful setting of the working point, defined by the demodulation phases and the off-sets (also depending on alignment), which is under investigation from a simulation point of view. We note here that the use of DarkF for simulating the interferometer in

this conditions seems problematic, for it defines the working point as the set of position which maximize the carrier power in the cavities, that it is certainly not the experimental condition. The sidebands' difference with respect to aberrations explains also the observed sidebands unbalancing versus tilts, described in the previous section: the Upper sidebands is cleaned with respect to misalignment, and its recycling gain is less affected by misalignment with respect to the Lower.
Recently J.Marque has suggested to abandon the Anderson Technique and to change the modulation frequency following the Ligo choice, i.e. to have the two sidebands equally far from the fundamental peaks (following Marque this frequency is called *nominal*). Whenever DarkF simulations have not checked Marque simulations, the previous observations on differences (and complications) due to different resonant conditions for the sidebands tend to support the choice of the nominal frequency. DarkF and Finesse have been extensively used to identify a good error signal for TCS. A quite remarkable result is reported in figure 2.1, where the simulated phase camera signal is compared with the measured one.

The simulations carried out with Finesse agree with DarkF and in particular have allowed to verify the good agreement not only of the shape of the wavefront but also of the amplitude of the measured signal on the pin-holed photodiode of the present phase camera, within 10 percent, measured as the value of negative peak in the phase camera signal. The simulation on cold interferometer shows a defocus term which is not compatible with the measured one because it has the right amplitude but inverted sign. For this case investigations are in progress to understand if the astigmatism of the input beam can be a source of this discrepancy. In case of hot interferometer the eventual input beam aberrations play a minor role and in this case the phase camera signal is in good agreement with the measured one, as

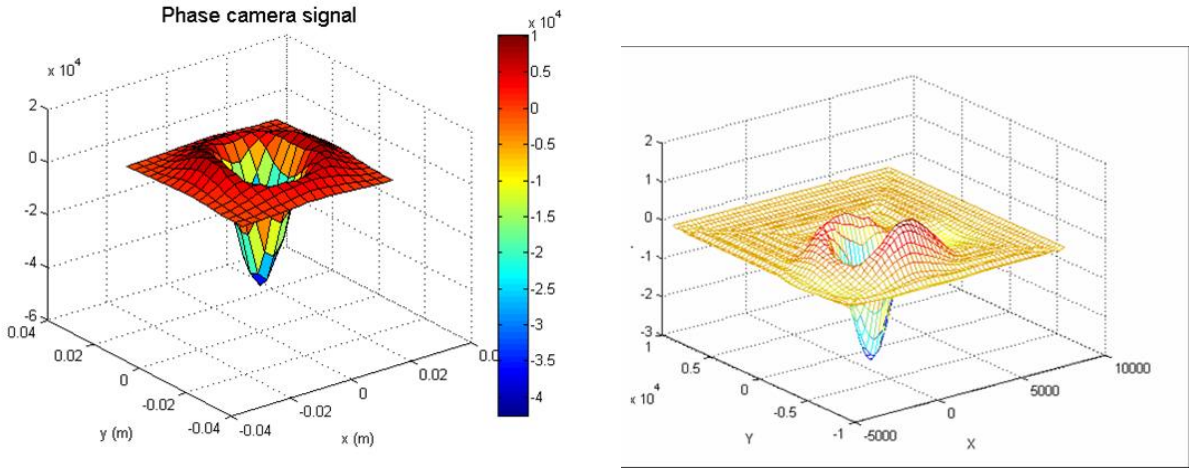

Figura 11: The simulated DarkF phase camera signal, on the left, and the measured one, on the right. The agreement on the shape of the wavefront is quite good. The complete evaluation has been performed with Finesse, see following figure

shown in figure Here we must point out that the actual phase camera does not distinguish between the two sidebands, so that the final signal is the sum of the two contributions.

For this reason the simulations of the phase camera signal are in good agreement with the measured one, while for the actual evaluation of each sidebands separately work remains to be done, as we discussed previously. Finally we note that also the wavefront where B2 is placed are affected by input mirror aberrations. A first work has been done to investigate the eventual possibility to use a phase camera (or a pin-hole mirror system) in this position to extract a second suitable error signal and diagonalize the TCS system. First indications on the use of B23f-pin-holed sgnal as second error signal are promising, but still not conclusive.

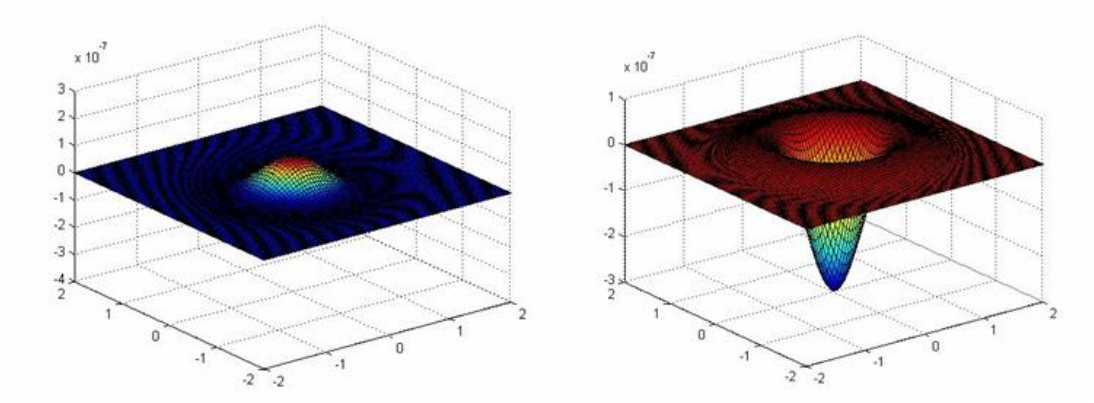

Figura 12: Finesse phase camera signal in cold and hot interferometer, where X and Y axes are in unity of waist. The vertical scale is the same of the measured signal. The input beam is taken to be perfect: investigations are currently carried out to uncertain if the disagreement with the measured one in case of cold interferometer is due to imperfections of input beam, not only in astigmatism but also in defocus. In case of hot interferometer the agreement is quite good

3 Analytical calculations and conclusion

The complexity of Virgo certainly is better described with the help of proper simulation tools then by analytical descriptions of aberrations. Nonetheless analytical calculations, typically performed with approximations, imposes a more intuitive understanding and can be useful as well. The calculations, reported in Appendix for sake of simplicity, have been used to choice the actual wavefront sensor for generating the TCS error signal, i.e. the phase camera. As it is known the phase camera demodulate the B5 photodiode signal at ω_m, scanning the wavefront by a pin-hole and a PZT system. As we noticed in section 1.3, the Science Mode "phase camera" will be a bull-eye equivalent photodiode system.

The motivation of the choice of the phase camera as the demodulation at ω_m of the B5 signal on the wavefront is contained in equation 47 of appendix, that we report here:

$$|\Psi_{BS}|^2_{\omega_m} = \left\{ \frac{8F}{\pi} \phi_1 Im \left[\hat{\Psi}^{CR}_{RC} \left(\hat{\Psi}^{+1\,*}_{RC} \right) \right] + 4Re \left[\hat{\Psi}^{CR}_{RC} \hat{\Psi}^{+1}_{RC} \right] \right\} \cos\left(\omega_m t\right) \qquad (3)$$

(See also the comments herein). In this approximations the sidebands aberration are taken to be equal, and in this case it it easily seen that the signal is proportional to the common mode input mirrors aberrations. We notice again that this signal is in good agreement with the DarkF simulations and the actualmeasurements, so that it is the one that will be used for TCS.

As stated in section 1.3, recently the question of using just one error signal or two has been raised again; this would imply the need of an error signal for differential mode. In the appendix, the differential mode is taken into account by the differential phase term $\phi^n_D(x,y)$, where the superscript n refers to the sidebands order. On this respect the most useful answer is contained in equation 39, that we report here:

$$Im(N) = -\frac{1}{4} \left\{ \cos(\phi_C(x,y)) \sin(\alpha) \cos\left(\phi_D(x,y)\right) \left[\frac{4F}{\pi} \left(\phi_1 - \phi_2\right) \right] - \right.$$

$$\left. \sin(\phi_C(x,y)) \cos(\alpha) \sin\left(\phi_D(x,y)\right) \left[\tfrac{2F}{\pi} \left(\eta_1 - \eta_2\right) \right] \right. \quad (4)$$

where it is shown that the quadrature signal at the output port of the interferometer, $B1p_Acq$ is proportional to that phase difference. This is actually the signal used in Ligo for differential mode and currently is the first candidate to be used also in Virgo, if needed.

On the other hand, we must understand if this signal could be masked by other interferometer imperfections (typically misalignments); simulation work is still under the way to understand if it is the case and if other signals could be more effective. Among them, presently a simple wavefront sensing on $B1_DC$ (a pin-hole system on DC) is under study as well as the wavefront sensing in B2, demodulating at 3f.

Appendix

A1 Recall of the fields in the interferometer and clarification of approximation

The notation of the field in the interferometer are reported in figure 10 at the last page of the paper. They are the same notations used by Erika D'ambrosio [3]. The field Ψ_{IN} is the result of the phase modulation of the initial Laser beam $E_L = E_0 e^{\imath\Omega t}$. It can be written as a superposition of carrier and sidebands:

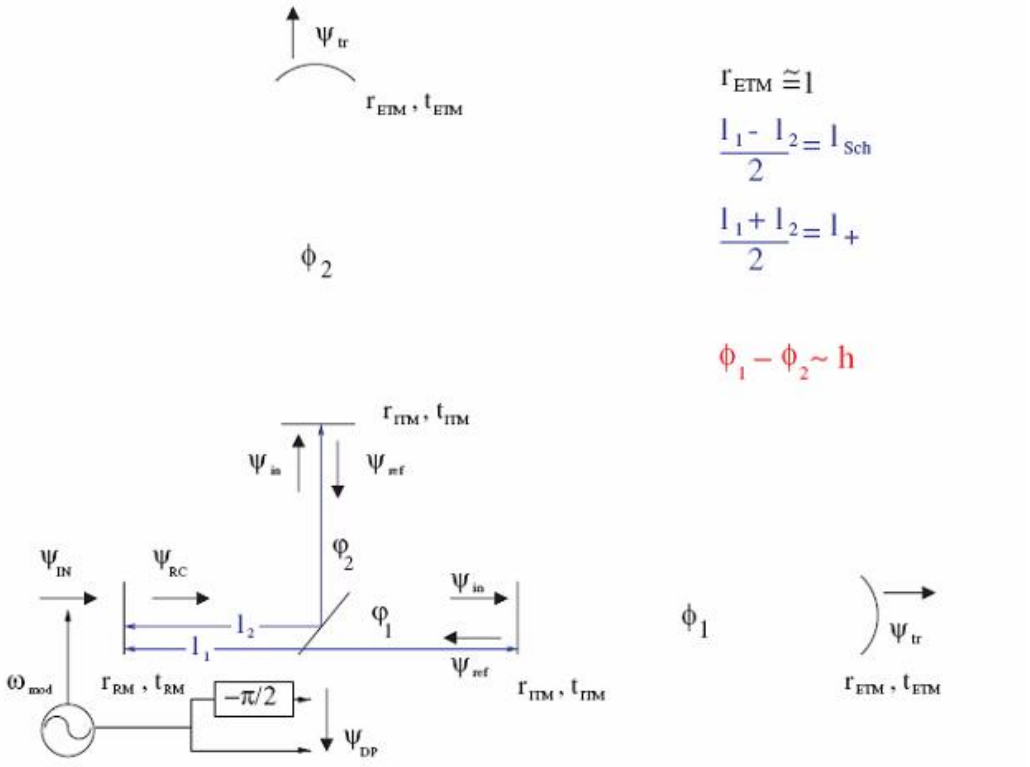

Figura 13: Interferometer fields nomenclature

$$\Psi_{IN} = E_0 e^{\imath(\Omega t + m\cos\omega_m t)} = \sum_{-\infty}^{+\infty} \Psi_{IN}^n \tag{5}$$

where m is the modulation depth and the ω_m is the modulation frequency. Each sidebands is thus:

$$\Psi_{IN}^n = E_L \left[\imath^{|n|} J_{|n|}(m) e^{\imath n\omega_m t}\right] \tag{6}$$

In this way each sidebands are indicated with the integer n and the carrier can be also indicate as the zero-order sideband. In the present draft we calculate the signals only at the 0,1,2 demodulation frequencies. In the calculation we neglect the contribution of the third harmonic; maybe this point should be reconsidered further.

Resonance situation for the various sidebands are reported in table1, where it is important to note that for odd n the sidebands are resonant while they are not for even n, except for the carrier.

A2 Signals in B5 and B1p in the ideal case and introduction to approximations

In this section we calculate the fields that can be detected with photodiodes B5 and B1p. Initially we calculate the fields in the interferometer and their intensity; the actual fraction of these signals that can be detected by a photodiode, for example due to BS reflectivity and other optics before the photodiodes, is discussed at the end of the section. With the notation of fig1 the field reflected by the arm is:

$$\Psi_{ref} \approx \Psi_{ref}^{CR} + \Psi_{ref}^{+1} + \Psi_{ref}^{-1} + \Psi_{ref}^{+2} + \Psi_{ref}^{-2} \tag{7}$$

The carrier field reflected by the arm 1,2 is:

$$\Psi_{ref1,2}^{CR} = \Psi_{in}^{CR}\left[1 + \frac{2\imath F}{\pi}\phi_{1,2} - \frac{F}{\pi}\eta_{1,2}\right] \tag{8}$$

The sidebands reflected fields are:

$$\Psi_{ref1,2}^{\pm 1,2} = -\Psi_{in}^{\pm 1,2} r_{ITM} e^{\imath\phi_{1,2}^{\pm 1,2}(x,y)} \tag{9}$$

Here the superscript 1,2 refers to the sideband while the subscript 1,2 refers to the arm of interferometer. The reflectivity of the mirror is approximated to unity. In order to calculate the signal it is useful to express the fields with the field in the recycling cavity. In this way the field just before recombining at the beam splitter can be written as:

The carrier field is:

$$\Psi_{ref1,2}^{CR} = \frac{1}{\sqrt{2}}\Psi_{RC}^{CR}\left[1 + \frac{2\imath F}{\pi}\phi_{1,2} - \frac{F}{\pi}\eta_{1,2}\right] e^{2\imath\omega(L_+ \pm L_{Sch})} \tag{10}$$

The 1 omega sidebands in the arm 1 are:

$$\Psi_{ref1}^{\pm 1} = \frac{1}{\sqrt{2}}\Psi_{RC}^{+1} e^{2\imath(\omega\pm\omega_m)(L_+ + L_{Sch})} e^{\imath\phi_1^{\pm 1}(x,y)} \tag{11}$$

While the 1 omega sidebands in the arm 2 are:

$$\Psi_{ref2}^{\pm 1} = \frac{1}{\sqrt{2}}\Psi_{RC}^{+1} e^{2\imath(\omega\pm\omega_m)(L_+ - L_{Sch})} e^{\imath\phi_2^{\pm 1}(x,y)} \tag{12}$$

Here $L_{Shc} = (L_1 - L_2)/2$ and $L_+ = (L_1 + L_2)/2$ indicate the Schnupp and the Recycling lengths respectively. In the same way it can be written the fields for the sidebands $|n| = 2$. Before to consider aberrations we recall the ideal optical conditions. Thus we impose dark fringe for the carrier at the output port $2\omega L_{Sch} = 2n\pi$ and carrier resonance condition in the recycling cavity $2\omega L_+ = 2n\pi$. Up to now

we have expressed all the fields in function of the field inside recycling cavity. This is the best procedure in our case because the measurements in DP and BS are indeed a measurement of the field in this cavity. Nevertheless it can be useful to express these fields starting from the fields Ψ_{IN} of the beam entering the interferometer. If t_{RM} and r_{RM} indicate the transmittivity and reflectivity of the recycling mirror.

$$\Psi_{RC}^{CR} = \frac{t_{RM}}{1 - r_{RM}} \Psi_{IN}^{CR} \tag{13}$$

$$\Psi_{RC}^{\pm 1} = \frac{t_{RM}}{1 + r_{RM}} \cos \frac{2\omega_m L_{Shc}}{c} e^{\pm 2\imath\omega_m L_+/c} \Psi_{IN}^{\pm 1} \tag{14}$$

and

$$\Psi_{RC}^{\pm 2} = \frac{t_{RM}}{1 + r_{RM} \cos \frac{2\omega_m L_{Shc}}{c} e^{\pm 4\imath\omega_m L_+/c}} \Psi_{IN}^{\pm 2} \tag{15}$$

Resonant condition for $|n| = 1$ sidebands is:

$$2\imath\omega_m L_+/c = (2n + 1)\pi \tag{16}$$

and all the $|n| = 1$ sidebands light exits the dark port if:

$$\cos 2\imath\omega_m L_{Shc}/c = r_{RM} \tag{17}$$

This condition makes not-resonant the $|n| = 2$ (and even) sidebands and resonant all the odds. It is now possible to express the field at the dark port DP and pick-off port PO, in our case the reflection of the field in arm 1 from the beam-splitter.

The field at the DP is (c=1):

$$\Psi_{DP} = \frac{1}{2}\left\{\Psi_{RC}^{CR}\left[\frac{2\imath F}{\pi}\left(\phi_1 - \phi_2\right) - \frac{F}{\pi}\left(\eta_1 - \eta_2\right)\right] + \right.$$

$$+ \imath \sin\left(2\omega_m L_{Sch}\right)\Psi_{RC}^{+1} - \imath \sin\left(2\omega_m L_{Sch}\right)\Psi_{RC}^{-1} +$$

$$+ \imath \sin\left(4\omega_m L_{Sch}\right)\Psi_{RC}^{+2} - \imath \sin\left(4\omega_m L_{Sch}\right)\Psi_{RC}^{-2} \quad (18)$$

while the field at the pick-off port BS is given by:

$$\Psi_{BS} = \frac{1}{\sqrt{2}}\left\{\Psi_{RC}^{CR}\left[1 + \frac{2\imath F}{\pi}\phi_1 - \frac{F}{\pi}\eta_1\right] - \Psi_{RC}^{\pm 1} - \Psi_{RC}^{\pm 2}\right\} \quad (19)$$

The time dependence of signals can be put in evidence indicating by $\Psi^n = \hat{\Psi^n} e^{\imath n\omega t}$; the field at the antisymmetric port DP (B1) and at the Beam Splitter port (B5) of the interferometer can then be calculated as (c =1):

$$\Psi_{DP} = \frac{1}{2}\left\{\Psi_{RC}^{CR}\left[\frac{2\imath F}{\pi}\left(\phi_1 - \phi_2\right) - \frac{F}{\pi}\left(\eta_1 - \eta_2\right)\right] + \right.$$

$$+ \imath\hat{\Psi}_{RC}^{+1} e^{\imath\omega_m t}\sin\left(2\omega_m L_{Sch}\right) +$$

$$\text{-}\imath\hat{\Psi}_{RC}^{-1} e^{-\imath\omega_m t}\sin\left(2\omega_m L_{Sch}\right) \quad (20)$$

And the field at the BS port:

$$\Psi_{BS} = \frac{1}{\sqrt{2}}\left\{\Psi_{RC}^{CR}\left[1 + \frac{2\imath F}{\pi}\phi_1 - \frac{F}{\pi}\eta_1\right] - \hat{\Psi}_{RC}^{\pm 1} e^{\pm\imath\omega_m t} - \hat{\Psi}_{RC}^{\pm 2} e^{\pm 2\imath\omega_m t}\right\} \quad (21)$$

Having discussed the main conditions regulating the work of the interferometer we can now recover the signals at the two photodiodes at the demodulation frequency of 1 omega. This is done for a better discussion in the following section when we will make a first analytical estimations of the effects of aberrations of input mirrors, to be eventually compared with non analytical simulations. Just to simplify the calculations we remember that in general the signal is $|\Psi|^2_{\omega_m} = (a + \imath b)e^{-\imath\omega_m t} + (a - \imath b)e^{-\imath\omega_m t}$, so that $|\Psi|^2_{\omega_m} = 2Re(a + \imath b)\cos(\omega_m t) - 2Im(a - \imath b)\sin(\omega_m t)$, and this

makes it convenient to calculate the quantity $N = (a + \imath b)$ and finally write that $|\Psi|^2_{\omega_m} = 2Re(N)\cos(\omega_m t) + 2Im(N)\sin(\omega_m t)$.

In the ideal case written up to now N_{DP} and N_{BS} are:

$$N_{DP} = \frac{1}{4}\left[\left[\frac{-2\imath F}{\pi}(\phi_1 - \phi_2) - \frac{F}{\pi}(\eta_1 - \eta_2)\right](-)\sin(2\omega_m L_{Sch})\,\Psi^{CR}_{RC}\Psi^{CR}_{-1} + \right.$$
$$\left. + \left[\frac{2\imath F}{\pi}(\phi_1 - \phi_2) - \frac{F}{\pi}(\eta_1 - \eta_2)\right](-)\sin(2\omega_m L_{Sch})\,\Psi^{CR}_{RC}\left(\Psi^{CR}_{+1}\right)^* \right. \quad (22)$$

In the ideal case the sidebands remain imaginary with respect to the carrier, so that we can continue to assume that $\Psi^{CR}_{+1} = \Psi^{CR}_{-1} = \imath\Psi^{CR}_{RC}$. We expect that this condition will be changed by aberrations. Calling $\alpha = (2\omega_m L_{Sch}$ the quantity N_{DP} becomes:

$$N_{DP} = \frac{1}{4}(-\imath\sin\alpha)\left[\frac{4\imath F}{\pi}(\phi_1 - \phi_2)\right] \quad (23)$$

As expected N_{DP} is imaginary so that the quadrature signal:

$$S_{DPq} = 2Im(N_{DP})\sin(\omega_m t) = \frac{1}{4}\sin\alpha\left[\frac{8F}{\pi}(\phi_1 - \phi_2)\right]\sin(\omega_m t) \quad (24)$$

is proportional only to the gravitational signal while, as expected, the in-phase signal $2Re(N_{DP})\cos(\omega_m t)$ is equal to zero.

In the same way the pick-off signal BS can be obtained considering that N_{BS} is equal to:

$$N_{BS} = \frac{1}{\sqrt{2}}\left\{\left[1 + \frac{2\imath F}{\pi}\phi_1 - \frac{F}{\pi}\eta_1\right]\Psi^{CR}_{RC}\left(\hat{\Psi}^{+1}_{RC}\right)^* + \left[1 + \frac{-2\imath F}{\pi}\phi_1 - \frac{F}{\pi}\eta_1\right]\Psi^{CR}_{RC}\left(\hat{\Psi}^{-1}_{RC}\right)\right\} \quad (25)$$

In the ideal case of sidebands imaginary and perfectly superposed to the carrier N_{BS} becomes simply:

$$N_{BS} = -\frac{1}{\sqrt{2}} \left\{ \frac{4F}{\pi} \phi_1 \right\} \tag{26}$$

As expected it is real so that the signal proportional to the phase difference between carrier and sidebands is recovered by the in-phase signal

$$S_{BSI} = 2Re(N_{BS}) \cos(\omega_m t) = -\frac{1}{\sqrt{2}} \left\{ \frac{8F}{\pi} \phi_1 \right\} \cos(\omega_m t) \tag{27}$$

while the quadrature signal is equal to zero.

Finally let us consider the signals at 2 omega. As it will be shown later the most important contribution is given by the interference of the $|n| = 1$ sidebands. In the ideal case as it is expected the two signals are a measure of the sidebands power distribution:

$$|\Psi_{DP}|^2_{2\omega_m} \approx \sin^2(2\omega_m L_{Sch})\, \hat{\Psi}^{+1}_{RC} \left(\hat{\Psi}^{-1}_{RC}\right)^* e^{2\imath\omega_m t} + \left(\hat{\Psi}^{+1}_{RC}\right)^* \hat{\Psi}^{-1}_{RC} e^{-2\imath\omega_m t} = 2\left[\hat{\Psi}^{\pm 1}_{RC} \left(\hat{\Psi}^{\pm 1}_{RC}\right)^*\right] \cos(2\omega_m t) \tag{28}$$

and

$$|\Psi_{BS}|^2_{2\omega_m} \approx \hat{\Psi}^{+1}_{RC} \left(\hat{\Psi}^{-1}_{RC}\right)^* e^{2\imath\omega_m t} + \left(\hat{\Psi}^{+1}_{RC}\right)^* \hat{\Psi}^{-1}_{RC} e^{-2\imath\omega_m t} = 2\left[\hat{\Psi}^{\pm 1}_{RC} \left(\hat{\Psi}^{\pm 1}_{RC}\right)^*\right] \cos(2\omega_m t) \tag{29}$$

A3 Signals in B5 and B1p in the non ideal case of input mirrors aberrations

Before to consider all the signals at the different modulation frequencies we consider the 1 omega signals, in which the main contribution is given by $|n| = 1$ sidebands interference with carrier. So for the moment we neglect the $|n| = 2$ sidebands in

our calculations. As we will see the $|n| = 2$ sidebands is nevertheless not important even for DC and 2 omega signals.

We first consider the DP signal, which is a bit less evident then the BS signal. Here we repeat the derivation already seen for the ideal case so to clarify the properties of the aberrations that we use. So we introduce the phases $\phi_{1,2}^{\pm 1}(x,y)$ acquired by the sideband ± 1 in reflection in the arm 1,2. Tacking into account of these phases the DP signal can be written as:

$$\Psi_{DP} = -\frac{1}{2}\left\{\Psi_{RC}^{CR}\left[1 + \frac{2\imath F}{\pi}\phi_1 - \frac{F}{\pi}\eta_1\right]e^{2\imath\omega(L_+ + L_{Sch})} + \right.$$
$$- \Psi_{RC}^{+1}e^{\imath\phi_1^{+1}(x,y)}e^{2\imath(\omega+\omega_m)(L_+ + L_{Sch})} - \Psi_{RC}^{-1}e^{\imath\phi_1^{-1}(x,y)}e^{2\imath(\omega-\omega_m)(L_+ + L_{Sch})} +$$
$$-\Psi_{RC}^{CR}\left[1 + \tfrac{2\imath F}{\pi}\phi_2 - \tfrac{F}{\pi}\eta_2\right]e^{2\imath\omega(L_+ - L_{Sch})} +$$
$$\left. + \Psi_{RC}^{+1}e^{\imath\phi_2^{+1}(x,y)}e^{2\imath(\omega+\omega_m)(L_+ - L_{Sch})} + \Psi_{RC}^{-1}e^{\imath\phi_2^{-1}(x,y)}e^{2\imath(\omega-\omega_m)(L_+ - L_{Sch})}\right\} \quad (30)$$

Ignoring the minus sign and the common phase term $e^{2\imath_+}$ the DP field can be written as:

$$\Psi_{DP} = \frac{1}{2}\left\{\Psi_{RC}^{CR}\left[1 + \frac{2\imath F}{\pi}\phi_1 - \frac{F}{\pi}\eta_1\right]e^{2\imath\omega L_{Sch}} + \right.$$
$$- \Psi_{RC}^{+1}e^{\imath\phi_1^{+1}(x,y)}e^{2\imath(\omega+\omega_m)L_{Sch}}e^{2\imath\omega_m L_+} - \Psi_{RC}^{-1}e^{\imath\phi_1^{-1}(x,y)}e^{2\imath(\omega-\omega_m)L_{Sch}}e^{-2\imath\omega_m L_+} +$$
$$-\Psi_{RC}^{CR}\left[1 + \tfrac{2\imath F}{\pi}\phi_2 - \tfrac{F}{\pi}\eta_2\right]e^{-2\imath\omega L_{Sch}} +$$
$$\left. + \Psi_{RC}^{+1}e^{\imath\phi_2^{+1}(x,y)}e^{-2\imath(\omega+\omega_m)L_{Sch}}e^{2\imath\omega_m L_+} + \Psi_{RC}^{-1}e^{\imath\phi_2^{-1}(x,y)}e^{-2\imath(\omega-\omega_m)L_{Sch}}e^{-2\imath\omega_m L_+}\right\} \quad (31)$$

Only now we finally re-impose the dark fringe condition: $2\omega L_{Sch} = 2n\pi$ so that

$$\Psi_{DP} = \frac{1}{2}\left\{\Psi_{RC}^{CR}\left[\frac{2\imath F}{\pi}(\phi_1 - \phi_2) - \frac{F}{\pi}(\eta_1 - \eta_2)\right] + \right.$$
$$\left. - \Psi_{RC}^{+1}e^{\imath\phi_1^{+1}(x,y)}e^{2\imath\omega_m L_{Sch}}e^{2\imath\omega_m L_+} - \Psi_{RC}^{-1}e^{\imath\phi_1^{-1}(x,y)}e^{-2\imath\omega_m L_{Sch}}e^{-2\imath\omega_m L_+} + \right.$$

$$+\ \Psi_{RC}^{+1}e^{\imath\phi_2^{+1}(x,y)}e^{-2\imath\omega_m L_{Sch}}e^{2\imath\omega_m L_+}+\Psi_{RC}^{-1}e^{\imath\phi_2^{-1}(x,y)}e^{-2\imath\omega_m L_{Sch}}e^{-2\imath\omega_m L_+} \quad (32)$$

Now we can start considering the aberrations and approximations that we can suppose: as first we suppose that the mean phases are equal to zero in reflection. This seems reasonable in that it should be just a rescaling of L_{Sch}. Nonetheless this condition could be discussed. With this condition true the conditions for resonance of sidebands are the usual $2\omega_m L_+ = (2n+1)\pi$ and the field at the dark port can be written as:

$$\Psi_{DP} = \frac{1}{2}\left\{\Psi_{RC}^{CR}\left[\frac{2\imath F}{\pi}\left(\phi_1-\phi_2\right)-\frac{F}{\pi}\left(\eta_1-\eta_2\right)\right]+\right.$$
$$+\ \Psi_{RC}^{+1}e^{\imath\phi_1^{+1}(x,y)}e^{2\imath\omega_m L_{Sch}}+\Psi_{RC}^{-1}e^{\imath\phi_1^{-1}(x,y)}e^{-2\imath\omega_m L_{Sch}}+$$
$$-\ \Psi_{RC}^{+1}e^{\imath\phi_2^{+1}(x,y)}e^{-2\imath\omega_m L_{Sch}}-\Psi_{RC}^{-1}e^{\imath\phi_2^{-1}(x,y)}e^{2\imath\omega_m L_{Sch}} \quad (33)$$

The phases can be divided in a common and differential phase such that $\phi_1^{\pm1}(x,y) = \phi_C^{\pm1}(x,y)+\phi_D^{\pm1}(x,y)$ and $\phi_2^{\pm1}(x,y) = \phi_C^{\pm1}(x,y)-\phi_D^{\pm1}(x,y)$ and the field becomes:

$$\Psi_{DP} = \frac{1}{2}\left\{\Psi_{RC}^{CR}\left[\frac{2\imath F}{\pi}\left(\phi_1-\phi_2\right)-\frac{F}{\pi}\left(\eta_1-\eta_2\right)\right]+\right.$$
$$+\ \Psi_{RC}^{+1}e^{\imath\phi_C^{+1}(x,y)}e^{2\imath\omega_m L_{Sch}}e^{\imath\phi_D^{+1}(x,y)}+\Psi_{RC}^{-1}e^{\imath\phi_C^{-1}(x,y)}e^{-2\imath\omega_m L_{Sch}}e^{\imath\phi_D^{-1}(x,y)}+$$
$$-\ \Psi_{RC}^{+1}e^{\imath\phi_C^{+1}(x,y)}e^{-2\imath\omega_m L_{Sch}}e^{-\imath\phi_D^{+1}(x,y)}-\Psi_{RC}^{-1}e^{\imath\phi_C^{-1}(x,y)}e^{2\imath\omega_m L_{Sch}}e^{-\imath\phi_D^{-1}(x,y)} \quad (34)$$

By some algebra we obtain:

$$\Psi_{DP} = \frac{1}{2}\left\{\Psi_{RC}^{CR}\left[\frac{2\imath F}{\pi}\left(\phi_1-\phi_2\right)-\frac{F}{\pi}\left(\eta_1-\eta_2\right)\right]+\right.$$
$$+\ \imath\hat{\Psi}_{RC}^{+1}e^{\imath\phi_C^{+1}(x,y)}e^{\imath\omega_m t}\sin\left(2\omega_m L_{Sch}+\phi_D^{+1}(x,y)\right)+$$
$$-\imath\hat{\Psi}_{RC}^{-1}e^{\imath\phi_C^{-1}(x,y)}e^{-\imath\omega_m t}\sin\left(2\omega_m L_{Sch}+\phi_D^{-1}(x,y)\right) \quad (35)$$

Now we consider that the sidebands are affected in the same way by reflection and impose $\phi_C^{+1}(x,y) = -\phi_C^{-1}(x,y) = \phi_C(x,y)$ and $\phi_D^{+1}(x,y) = -\phi_D^{-1}(x,y) = \phi_D(x,y)$.

Of course here we are neglecting the effects of differences in sidebands.

In this way we can write:

$$\Psi_{DP} = \frac{1}{2}\left\{\Psi_{RC}^{CR}\left[\frac{2\imath F}{\pi}\left(\phi_1-\phi_2\right)-\frac{F}{\pi}\left(\eta_1-\eta_2\right)\right]+\right.$$
$$+\ \imath\hat{\Psi}_{RC}^{+1}e^{\imath\phi_C(x,y)}e^{\imath\omega_m t}\left[\sin\left(2\omega_m L_{Sch}\right)\cos\left(\phi_D(x,y)\right)+\cos\left(2\omega_m L_{Sch}\right)\sin\left(\phi_D(x,y)\right)\right]$$
$$-\imath\hat{\Psi}_{RC}^{-1}e^{-\imath\phi_C^{-1}(x,y)}e^{-\imath\omega_m t}\left[\sin\left(2\omega_m L_{Sch}\right)\cos\left(\phi_D(x,y)\right)-\cos\left(2\omega_m L_{Sch}\right)\sin\left(\phi_D(x,y)\right)\right] \quad (36)$$

In this case the quantity N is given by:

$$N = \frac{1}{4}\left\{\Psi_{RC}^{CR}\left(\hat{\Psi}_{RC}^{+1}\right)^*\left[\frac{2\imath F}{\pi}\left(\phi_1-\phi_2\right)-\frac{F}{\pi}\left(\eta_1-\eta_2\right)\right](-\imath)e^{-\imath\phi_C(x,y)}\left[\sin(\alpha)\cos\left(\phi_D(x,y)\right)\right]+\right.$$
$$\Psi_{RC}^{CR}\left(\hat{\Psi}_{RC}^{+1}\right)^*\left[\tfrac{2\imath F}{\pi}\left(\phi_1-\phi_2\right)-\tfrac{F}{\pi}\left(\eta_1-\eta_2\right)\right](-\imath)e^{-\imath\phi_C(x,y)}\left[\cos(\alpha)\sin\left(\phi_D(x,y)\right)\right]+$$
$$\Psi_{RC}^{CR}\hat{\Psi}_{RC}^{-1}\left[\tfrac{-2\imath F}{\pi}\left(\phi_1-\phi_2\right)-\tfrac{F}{\pi}\left(\eta_1-\eta_2\right)\right](-\imath)e^{-\imath\phi_C(x,y)}\left[\sin(\alpha)\cos\left(\phi_D(x,y)\right)\right]+$$
$$\Psi_{RC}^{CR}\hat{\Psi}_{RC}^{-1}\left[\tfrac{-2\imath F}{\pi}\left(\phi_1-\phi_2\right)-\tfrac{F}{\pi}\left(\eta_1-\eta_2\right)\right](\imath)e^{-\imath\phi_C(x,y)}\left[\cos(\alpha)\sin\left(\phi_D(x,y)\right)\right] \quad (37)$$

The sidebands are almost imaginary with respect to carrier so that it is convenient to write them as: $\hat{\Psi}_{RC}^{\pm1} = \imath\hat{\Psi}_{RC}^{\pm1}$. An eventual common phase of the two carrier can be considered comprised in $\phi_C(x,y)$.

$$N = \frac{1}{4}e^{-\imath\phi_C(x,y)}\left\{\left[\frac{2\imath F}{\pi}\left(\phi_1-\phi_2\right)-\frac{F}{\pi}\left(\eta_1-\eta_2\right)\right](-1)\left[\sin(\alpha)\cos\left(\phi_D(x,y)\right)\right]+\right.$$
$$\left[\tfrac{2\imath F}{\pi}\left(\phi_1-\phi_2\right)-\tfrac{F}{\pi}\left(\eta_1-\eta_2\right)\right](-1)\left[\cos(\alpha)\sin\left(\phi_D(x,y)\right)\right]+$$
$$\left[\tfrac{-2\imath F}{\pi}\left(\phi_1-\phi_2\right)-\tfrac{F}{\pi}\left(\eta_1-\eta_2\right)\right](+1)\left[\sin(\alpha)\cos\left(\phi_D(x,y)\right)\right]+$$
$$\left[\tfrac{-2\imath F}{\pi}\left(\phi_1-\phi_2\right)-\tfrac{F}{\pi}\left(\eta_1-\eta_2\right)\right](-1)\left[\cos(\alpha)\sin\left(\phi_D(x,y)\right)\right] \quad (38)$$

And then N is equal to:

$$N = \frac{1}{4} e^{-\imath\phi_C(x,y)} \left\{ \left[\frac{-4\imath F}{\pi} (\phi_1 - \phi_2) \right] \sin(\alpha) \cos\left(\phi_D(x,y)\right) + \left[\frac{2F}{\pi} (\eta_1 - \eta_2) \right] \cos(\alpha) \sin\left(\phi_D(x,y)\right) \right\} \tag{39}$$

Finally we obtain:

$$N = \frac{1}{4} \left[\cos(\phi_C(x,y)) - \imath \sin(\phi_C(x,y))\right] \left\{ \left[\frac{-4\imath F}{\pi} (\phi_1 - \phi_2) \right] \sin(\alpha) \cos\left(\phi_D(x,y)\right) + \left[\frac{2F}{\pi} (\eta_1 - \eta_2) \right] \cos(\alpha) \right. \tag{40}$$

The real part of N is then equal to:

$$Re(N) = \frac{1}{4} \left\{ \cos(\phi_C(x,y)) \cos(\alpha) \sin\left(\phi_D(x,y)\right) \left[\frac{2F}{\pi} (\eta_1 - \eta_2) \right] - \right.$$
$$\sin(\phi_C(x,y)) \sin(\alpha) \cos\left(\phi_D(x,y)\right) \left[\tfrac{4F}{\pi} (\phi_1 - \phi_2) \right] \tag{41}$$

and in the same way, for Im(N) it can be found:

$$Im(N) = -\frac{1}{4} \left\{ \cos(\phi_C(x,y)) \sin(\alpha) \cos\left(\phi_D(x,y)\right) \left[\frac{4F}{\pi} (\phi_1 - \phi_2) \right] - \right.$$
$$\sin(\phi_C(x,y)) \cos(\alpha) \sin\left(\phi_D(x,y)\right) \left[\tfrac{2F}{\pi} (\eta_1 - \eta_2) \right] \tag{42}$$

These are the most important expressions to observe to understand what signal can be interesting for our purpose. The signal proportional to the Im(N) is in quadrature with respect to the modulation signal and it is what Virgo calls In Phase for historical reasons and it is the signal of the gravitational signal. On the opposite, what we call In quadrature is the signal proportional to Re(N) which is in phase with the modulation signal.

The opposite is done by Ligo: they call in phase what is in phase and in quadrature what is in quadrature (a typical rough and incomprehensible way of doing of Americans!).

One of the 2 signals that Ligo uses as an error signal for thermal compensation of the input mirrors radius of curvature is what they called AS_I. From what we said this signal corresponds to the physical in phase signal i.e. what it obtained by Re(N). In our calculations this signal is to the leading order proportional to the differential aberrations acquired by the sidebands: this sounds reasonable whenever it must be better understood.

For what concerns the signal that can be taken at the pick-off port the situation is much more clear. We also write the signals in DC and 1 and 2 omega due to the fact that maybe a photodiode pixellated will be used here, that could be centered with DC signal and to compare the various contributions.

For the D.C. signal it is easily obtained:

$$|\Psi_{BS}|^2_{DC} = \left|\Psi^{CR}_{RC}\right|^2 + \left|\Psi^{\pm 1}_{RC}\right|^2 + \left|\Psi^{\pm 2}_{RC}\right|^2 \tag{43}$$

The major contribution to the signal at the modulation frequency is given by:

$$|\Psi_{BS}|^2_{\omega_m} = -\hat{\Psi}^{CR}_{RC}\left(\hat{\Psi}^{+1}_{RC}\right)^*\left(1+\frac{2\imath F}{\pi}\phi_1 - \frac{F}{\pi}\eta_1\right)e^{-\imath\omega_m t} - \left(\hat{\Psi}^{CR}_{RC}\right)^*\hat{\Psi}^{+1}_{RC}\left(1-\frac{2\imath F}{\pi}\phi_1 - \frac{F}{\pi}\eta_1\right)e^{\imath\omega_m t} +$$
$$\hat{\Psi}^{CR}_{RC}\left(\hat{\Psi}^{-1}_{RC}\right)^*\left(1+\tfrac{2\imath F}{\pi}\phi_1 - \tfrac{F}{\pi}\eta_1\right)e^{\imath\omega_m t} + (44)$$

While the major contribution to the signal at the double of the modulation frequency is given by:

$$|\Psi_{BS}|^2_{2\omega_m} = \hat{\Psi}^{+1}_{RC}\left(\hat{\Psi}^{-1}_{RC}\right)^* e^{2\imath\omega_m t} + \left(\hat{\Psi}^{+1}_{RC}\right)^*\hat{\Psi}^{-1}_{RC}e^{-2\imath\omega_m t} +$$
$$+\hat{\Psi}^{CR}_{RC}\left(\hat{\Psi}^{+2}_{RC}\right)^*\left(1+\tfrac{2\imath F}{\pi}\phi_1 - \tfrac{F}{\pi}\eta_1\right)e^{-2\imath\omega_m t} - \left(\hat{\Psi}^{CR}_{RC}\right)^*\hat{\Psi}^{+2}_{RC}\left(1-\tfrac{2\imath F}{\pi}\phi_1 - \tfrac{F}{\pi}\eta_1\right)e^{2\imath\omega_m t} +$$
$$-\hat{\Psi}^{CR}_{RC}\left(\hat{\Psi}^{-2}_{RC}\right)^*\left(1+\tfrac{2\imath F}{\pi}\phi_1 - \tfrac{F}{\pi}\eta_1\right)e^{2\imath\omega_m t} - \left(\hat{\Psi}^{CR}_{RC}\right)^*\hat{\Psi}^{-2}_{RC}\left(1-\tfrac{2\imath F}{\pi}\phi_1 - \tfrac{F}{\pi}\eta_1\right)e^{-2\imath\omega_m t} \tag{45}$$

In the previous equation we have neglected the contribution given from the interference of the $|n| = 1$ with $|n| = 2$ sidebands at the 1ω signal, because it is negligible. As a further approximation consider the sidebands to be equal and take $\hat{\Psi}_{RC}^{CR}$ real. With these approximation we can write, for the power in DC, at 1 and 2 ω:

$$|\Psi_{BS}|_{DC}^2 \approx \left|\Psi_{RC}^{CR}\right|^2 \tag{46}$$

This equation just recalls that the DC signal out from the BS is essentially the power of carrier. In a pixellated photodiode it can be used to center the beam on the photodiode in the same way as it is presently discussed for the alignment photodiodes. We now write the signal at the modulation frequency following the previous approximations, but pointing out that the sidebands could take a real term, equivalent to a modulation not only in phase but also, much smaller, in amplitude. We let this term written not for a present comment but for eventual discussion. Finally the loss $\frac{F}{\pi}\eta$ is neglected respect to unity. With this considerations the signal at the modulation frequency is:

$$|\Psi_{BS}|_{\omega_m}^2 = \left\{\frac{8F}{\pi}\phi_1 Im\left[\hat{\Psi}_{RC}^{CR}\left(\hat{\Psi}_{RC}^{+1\,*}\right)\right] + 4Re\left[\hat{\Psi}_{RC}^{CR}\hat{\Psi}_{RC}^{+1}\right]\right\}\cos\left(\omega_m t\right) \tag{47}$$

From this equation it is recalled that the main signal at the modulation frequency in phase is the phase difference between carrier and sideband(s). (We remember that sidebands are presently taken to be equal). This is the signal that in our opinion seems the best to recover aberrations of the sidebands with respect to the carrier: indeed aberrations will produce a first order error signal in phase difference while they will produce a second order effect in power. Nevertheless the power of the sidebands can be detected at the double of the modulation frequency. Indeed the power at $2\omega_m$ can be calculated as:

$$|\Psi_{BS}|^2_{2\omega_m} \approx \hat{\Psi}^{+1}_{RC}\left(\hat{\Psi}^{-1}_{RC}\right)^* e^{2\imath\omega_m t} + \left(\hat{\Psi}^{+1}_{RC}\right)^* \hat{\Psi}^{-1}_{RC} e^{-2\imath\omega_m t} = 2\left[\hat{\Psi}^{\pm 1}_{RC}\left(\hat{\Psi}^{\pm 1}_{RC}\right)^*\right]\cos\left(2\omega_m t\right) \tag{48}$$

Where again we have supposed the two sidebands equal and we have neglected the contribution arising from the interference of carrier and $|n| = 2$ sidebands. Indeed this last terms are of the order $\hat{\Psi}^{CR}_{RC}\hat{\Psi}^{\pm 2}_{RC} \approx \sqrt{G^{CR}} t_{RM} m^2 < \hat{\Psi}^{1}_{RC}\hat{\Psi}^{-1}_{RC} \approx G^{\pm 1} m^2$ with $F^{\pm 1}m^2$ equal to the gain of the recycling cavity for the $|n| = 1$ sidebands. This last gain is measured to be 20 while the product of the carrier recycling gain and recycling mirror transmittivity $40 * 0.04 = 1.6$ is a bit more than one order of magnitude less and allows us to neglect the contribution. It is also interesting to note that if the sidebands are not equal or are phase shifted one with respect to the other then a signal in quadrature arise at the double of the modulation frequency that could be considered eventually as an error signal for their differences.

With the same approximations the DC signal at the output port DP can be expressed as:

$$|\Psi_{DP}|^2_{DC} \approx \left|\Psi^{CR}_{RC}\right|^2 (1 - \Gamma) + \alpha^2 \left(\left|\Psi^{+1}_{RC}\right|^2 + \left|\Psi^{-1}_{RC}\right|^2\right) \tag{49}$$

where Γ = Carrier contrast, $\alpha = \sin\left(\frac{2\omega_m L_{Shc}}{c}\right)$. These quantities must be measured for the new laser power.

References

[1] http://wwwcascina.virgo.infn.it/collmeetings/DMwebpages/ Anderson/Nominal Frequency - J. Marque presentation November 2007

[2] http://wwwcascina.virgo.infn.it/collmeetings/DMwebpages/ Thermal effects and Correction - M. Laval presentation on LSC Virgo meeting May 2007

[3] E. D'ambrosio: "Study of the different responsive behaviour of the sidebands in Ligo 1", Class. Quant. Grav. **21** (2004) S1113